Earth and Planetary Science Letters 467 (2017) 79–88

Contents lists available at ScienceDirect

Earth and Planetary Science Letters

www.elsevier.com/locate/epsl

Asymmetry in growth and decay of the geomagnetic dipole revealed in seafloor magnetization

Margaret S. Avery *, Jeffrey S. Gee, Catherine G. Constable

Scripps Institution of Oceanography, University of California, San Diego, La Jolla, CA 92093, USA

ARTICLE INFO

Article history:
Received 7 September 2016
Received in revised form 9 March 2017
Accepted 14 March 2017
Available online xxxx
Editor: B. Buffett

Keywords:
paleomagnetic field strength
dipole moment variations
near-bottom marine magnetic anomalies

ABSTRACT

Geomagnetic intensity fluctuations provide important constraints on time-scales associated with dynamical processes in the outer core. PADM2M is a reconstructed time series of the 0–2 Ma axial dipole moment (ADM). After smoothing to reject high frequency variations PADM2M's average growth rate is larger than its decay rate. The observed asymmetry in rates of change is compatible with longer term diffusive decay of the ADM balanced by advective growth on shorter time scales, and provides a potentially useful diagnostic for evaluating numerical geodynamo simulations. We re-analyze the PADM2M record using improved low-pass filtering to identify asymmetry and quantify its uncertainty via bootstrap methods before applying the new methodology to other kinds of records. Asymmetry in distribution of axial dipole moment derivatives is quantified using the geomagnetic skewness coefficient, s_g. A positive value indicates the distribution has a longer positive tail and the average growth rate is greater than the average decay rate. The original asymmetry noted by Ziegler and Constable (2011) is significant and does not depend on the specifics of the analysis.

A long-term record of geomagnetic intensity should also be preserved in the thermoremanent magnetization of oceanic crust recovered by inversion of stacked profiles of marine magnetic anomalies. These provide an independent means of verifying the asymmetry seen in PADM2M. We examine three near-bottom surveys: a 0 to 780 ka record from the East Pacific Rise at 19°S, a 0 to 5.2 Ma record from the Pacific Antarctic Ridge at 51°S, and a chron C4Ar–C5r (9.3–11.2 Ma) record from the NE Pacific. All three records show an asymmetry similar in sense to PADM2M with geomagnetic skewness coefficients, $s_g > 0$. Results from PADM2M and C4Ar–C5r are most robust, reflecting the higher quality of these geomagnetic records. Our results confirm that marine magnetic anomalies can carry a record of the asymmetric geomagnetic field behavior first found for 0–2 Ma in PADM2M, and show that it was also present during the earlier time interval from 9.3–11.2 Ma.

1. Introduction

Motion of liquid-iron in Earth's outer core generates the geomagnetic field, which exhibits directional and intensity changes on a broad array of timescales. These variations are recorded in newly forming igneous rocks and sediments on land and beneath the seafloor where numerous paleomagnetic and marine magnetic anomaly studies have been conducted. The resulting data can be used to constrain global time-varying models of past field behavior.

Much of our understanding of geomagnetic field variations over the past few million years comes from paleofield direction and relative paleointensity (RPI) variations recorded by marine sediments (Roberts et al., 2013; Tauxe and Yamazaki, 2015; Valet and Fournier, 2016). Absolute paleointensity data derived from igneous rocks are necessary to calibrate the RPI. Polarity reversals occur aperiodically every few hundred thousand years and are accompanied by lows in intensity. Directional excursions are incomplete reversals, also featuring low field strength, which occur more frequently than reversals but are not always global in extent. Within polarity chrons there are also globally coherent higher frequency variations in paleointensity. These higher frequency variations are evident in sedimentary RPI records and are sometimes observed as globally coherent tiny-wiggles in marine magnetic anomaly records (Cande and LaBrecque, 1974; Cande and Kent, 1992b). Marine magnetic anomaly records provide a robust record of polarity reversals (Cande and Kent, 1995) and high quality anomaly data are also a viable alternative for studying geomagnetic intensity variations (Gee et al., 2000).

* Corresponding author.
E-mail address: msavery@ucsd.edu (M.S. Avery).

http://dx.doi.org/10.1016/j.epsl.2017.03.020

The temporal resolution of individual time series of RPI and magnetic anomaly data are determined locally by sedimentation or spreading rate, respectively, and by other geological and environmental factors that may influence the quality of the geomagnetic record. When multiple records are combined to study regional or global variations the limiting factor is the ability to match the chronology across records.

In one example of a 0–4 Ma record from sediments from the equatorial Pacific sampled during Leg 138 of the Ocean Drilling Program, Valet and Meynadier (1993) observed a saw-toothed intensity variation. The intensity decreased gradually over the course of a polarity interval (with a characteristic relaxation time of ∼0.5 Myr) then rapidly rebounded over a few thousand years after the field reversed direction, restarting the cycle. The saw-tooth intensity pattern is not observed in all sedimentary records, nor is it universally accepted as caused by field behavior. For example, the 0.5 Myr relaxation timescale observed by Valet and Meynadier (1993) may be due to a viscous remanent magnetization (Kok and Tauxe, 1996a, 1996b); see Tauxe and Yamazaki (2015) for a review and discussion. However, differing rates of growth and decay before and after a reversal have been observed in other sedimentary records and stacks, including Sint-2000 (Valet et al., 2005) where a decrease in dipole strength is observed over 60–80 kyr, followed by a recovery period of only a few thousand years.

A global view of geomagnetic field strength over 0–2 Ma is provided by PADM2M (Ziegler et al., 2011), a reconstruction of ADM variations using 76 time series of sedimentary RPI and more than 5000 absolute paleointensity data from igneous and archaeological materials. The restriction to ADM variations is a consequence of chronological constraints which determine the temporal resolution, combined with limited geographical coverage and an absence of complementary directional information in the data compilation. PADM2M provides a robust measure of ADM variations at about 10 kyr temporal resolution, and yields an average ADM for the past 2 Ma of 5.3×10^{22} Am^2 with a standard deviation of 1.5×10^{22} Am^2. The average for the Brunhes chron (0–780 ka, 6.23×10^{22} Am^2) is higher than during the Matuyama chron (780 ka–1.77 Ma, 4.8×10^{22} Am^2).

PADM2M offers the possibility of identifying characteristic time scales associated with specific aspects of core dynamics. Ziegler and Constable (2011) examined long-term (25–150 kyr) variations of PADM2M and its derivative, and found an asymmetry in the distribution of growth and decay rates. When variations shorter than 36 kyr are smoothed out in the PADM2M model, they found an average growth rate that is 20% larger than the average decay rate: the field spends 54% of its time decaying compared with 46% growing. This behavior is not limited to intervals immediately surrounding field reversals. Ziegler and Constable (2011) attributed this asymmetry to physical processes occurring on different timescales, a long decay timescale associated with diffusive losses in ADM, and the more rapid growth related to a temporally filtered view of advective processes.

A simplified cartoon of an ADM model with this kind of behavior is plotted in Fig. 1. Age is specified as negative time and time progresses from left to right, so negative slopes are periods of decay and positive slopes are periods of field growth. This convention allows straightforward comparison with advancing time steps in geodynamo simulation results. The field spends more time decaying than growing, but the rates of growth are greater in magnitude.

The rate of change of the geomagnetic field is controlled by contributions from diffusion and advection in the outer core, as described by the first and second terms, respectively, on the right hand side of the magnetic induction equation:

$$\frac{\partial \mathbf{B}}{\partial t} = \eta \nabla^2 \mathbf{B} + \nabla \times (\mathbf{u} \times \mathbf{B}), \quad (1)$$

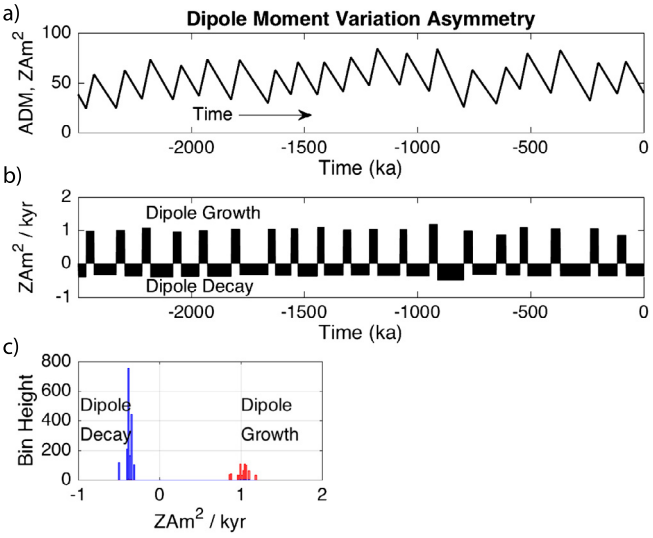

Fig. 1. a) A cartoon of ADM time variations displaying asymmetry between growth and decay rates. b) The first derivative of the ADM model in a) evaluated every 1 kyr. c) Histogram showing the distribution of the derivatives from b).

where t is time, $\mathbf{B}$ is magnetic field, η is magnetic diffusivity, and $\mathbf{u}$ is core fluid velocity. The longer, slower decay of the dipole suggests periods where the field is dominated by diffusion, and the shorter, faster periods of growth suggest advection is (on average) acting to increase the dipole strength. The timescale of diffusion for the ADM is characterized by $t_d = \frac{r_o^2}{\pi^2 \eta} \sim 54$ kyr, the e-folding time for dipole magnetic field decay if fluid motion in the outer core ceased (Backus et al., 1996). Here r_o is the outer core radius (3.5×10^6 m) and η is the magnetic diffusivity (0.72 m^2/s, Pozzo et al., 2012). The advection timescale is described by the time it takes fluid to move from the inner core boundary to the core mantle boundary: $t_a = d/U \sim 200$ yr, where $d = r_o - r_i$ the outer core thickness (2.2×10^6 m) and U is the characteristic outer core fluid velocity ($\sim 5 \times 10^{-4}$ m/s, Holme, 2015).

In what follows we first evaluate the robustness of the initial asymmetry result from PADM2M presented by Ziegler and Constable (2011) through development of improved analysis methods that sharpen the earlier results and provide uncertainty estimates (Section 2). We explore the possibility of identifying the asymmetry in rate of change of the thermoremanent magnetization (TRM) of the oceanic crust and the associated marine magnetic anomalies. Seafloor magnetization recovered from inversion of stacks of near-bottom marine magnetic anomalies are considered as a proxy for RPI and used as an independent means of assessing the asymmetry seen in PADM2M (Section 3). Seafloor magnetization records that span a similar time period (0–780 ka and 0–5.2 Ma) to that covered by PADM2M are analyzed using the same techniques. To test the persistence through time of the asymmetric behavior, we also examine high quality near-bottom marine magnetic anomaly records from chrons C4Ar–C5r that record field behavior from 9.3–11.2 Ma. The asymmetry between growth and decay rates observed in PADM2M is robust, and the peak asymmetry is most evident when fluctuations faster than ∼50 kyr are filtered out. All three records show an asymmetry between growth and decay similar in sense to PADM2M: the distribution of ADM derivatives has a longer positive tail. We discuss the robustness of these results in the context of the greater reliability of the records provided by PADM2M and C4Ar–C5r, compared with the younger marine magnetic anomaly records.

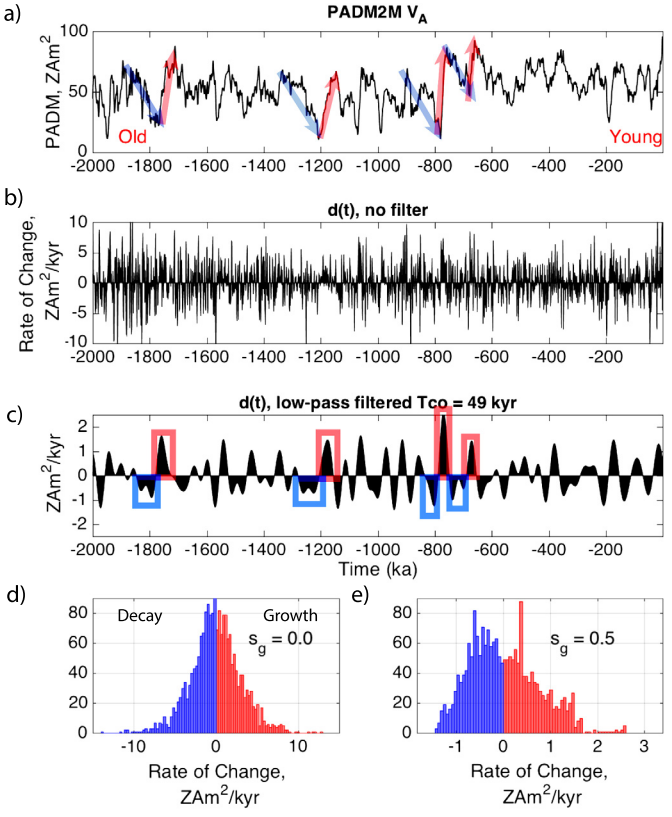

Fig. 2. An example of asymmetry between growth and decay rate observed after low-pass filtering. a) Unfiltered PADM2M timeseries (1 ZAm^2 = 10^{21} Am^2) and b) its first derivative evaluated at 1 kyr intervals, c) is an example of a low-pass filtered version of the derivatives of PADM2M, using the methods described in the text, d) shows the histogram of values for the unfiltered time series in b), with geomagnetic skewness coefficient $s_g = 0.0$, and e) same as d) but for the filtered rates of change given in c) with $s_g = 0.5$. (For interpretation of the references to color in this figure, the reader is referred to the web version of this article.)

2. Identifying asymmetry in time series of paleointensity

We outline the methods used to identify asymmetry in growth and decay rate, using PADM2M as an illustration (Fig. 2). The blue and red arrows in Fig. 2a highlight some readily identifiable intervals where the dipole moment is on average decaying slowly and is followed by a period of more rapid growth. To study these in more detail we evaluate the rate of change with time before (Fig. 2b) and after (Fig. 2c) low-pass filtering of the time derivative of PADM2M to remove variations at frequencies higher than a cutoff frequency of $f_{co} = 1/T_{co}$ (that is for periods shorter than T_{co}). The associated distributions of rates of decay are provided in Fig. 2d and Fig. 2e. In the unfiltered series the time spent growing and decaying is well balanced, but applying a low-pass filter uncovers an imbalance in the rates of change: positive values, which correspond to a growing dipole, are larger on average and occur less frequently than negative rates of decay. As we show below, the maximum asymmetry is found at a cutoff period of $T_{co} = 49$ kyr.

The ADM (V_A) is expressed as a spline variation in time. We calculate the analytical derivative

$$d(t) = \frac{dV_A}{dt}, \tag{2}$$

and evaluate it at uniformly spaced intervals of 1 kyr over 0–2 Ma as the starting point for our analysis. We used a Parks–McClellan equiripple low-pass filter as implemented in MatLab routine firpm (Parks and McClellan, 1972), which produces a sharp exclusion of variations below the specified cutoff period T_{co}. As discussed in the supplementary material (Section 1.1) it is more effective than the method previously used by Ziegler and Constable (2011). By varying T_{co}, from 10 to 150 kyr we can study how the asymmetry varies as a function of successively longer timescales. A diagnostic for the level of asymmetry in growth and decay, is provided by the skewness in the distribution of decay rates, which we call the geomagnetic skewness.

In a skewed or asymmetric distribution (Fig. 2e) the average rate of decay is different from the average rate of growth, and the field spends more time in one state than the other. A robust estimate of asymmetry is provided by the geomagnetic skewness coefficient, s_g, for the distribution of dipole field derivatives, d_i. The geomagnetic skewness of a distribution is the third moment about the mean. The geomagnetic skewness coefficient, s_g, is rendered dimensionless through normalization by the standard deviation cubed, and is convenient for making comparisons across the various distributions considered later.

$$s_g = \frac{\frac{1}{m}\sum_{i=1}^{m}\left(d_i - \overline{d}\right)^3}{\left(\sqrt{\frac{1}{m}\sum_{i=1}^{m}\left(d_i - \overline{d}\right)^2}\right)^3} \tag{3}$$

The asymmetry manifests as a distribution of derivatives with a longer positive tail, $s_g > 0$. Figs. 2d and e show two example distributions of rates of change: in Fig. 2d, the unfiltered PADM2M record exhibits no asymmetry ($s_g = 0.0$), while in Fig. 2e there is asymmetry between growth and decay rates and $s_g = 0.5 \pm 0.1$, corresponding to more time spent in decay mode and shorter intervals of more rapid growth. The uncertainty value is estimated with a delete-one jackknife resampling of the original 76 records making up PADM2M, and using the variability in geomagnetic skewness coefficient across the various pseudo-sampled models to calculate the standard error, $\widehat{se}_{jack}$, (see the supplement Section 1.2). The updated results for PADM2M are shown in Fig. 3 and reported in Table 1. This is the same result found by Ziegler and Constable (2011) although they parameterize the asymmetry with the percentages of time spent growing and decaying, which are unequal. It is important to note that, because of the direction of the time axis in our study, field decay corresponds to negative derivatives while in Ziegler and Constable (2011) field decay corresponded to positive derivatives. The geomagnetic skewness coefficient has the advantage of containing information about the mean rate of change making it a more robust estimator than the percentage growth criterion used previously.

Details about the different filtering methods can be found in the supplementary materials Section 1.1. Here we simply note that the method used here simplifies specification of T_{co}. The Parks–McClellan equiripple low-pass filter we used has a sharper frequency response than the spline method previously used by Ziegler and Constable (2011) (see Figure S1). The improved low-pass filtering does not affect the basic conclusion that there is asymmetry in the distribution of growth and decay. For PADM2M the peak magnitude of the geomagnetic skewness coefficient ($s_g = 0.5$) occurs at $T_{co} = 49$ kyr (see Table 1).

Table 1
Summary of asymmetry geomagnetic skewness results. n = number of sedimentary records (PADM2M) or anomaly profiles, R_+ = period range of significantly positive s_g. Chron C5 refers to the Northeastern Pacific Chron C5 record. Less robust results from the Brunhes 19°S East Pacific Rise (EPR) record and 0–5.2 Ma 51°S Pacific Antarctic Ridge (PAR) record are shown in italics.

Study	n	peak s_g	T_{co} of peak s_g	R_+ in T_{co}
PADM2M	76	0.5	49 kyr	15–107 kyr
Chron C5 43°N	12	0.5	39 kyr	15–107 kyr
EPR 19°S	*8*	*1.1*	*15 kyr*	*<25 kyr and >39 kyr*
PAR 51°S	*3*	*0.7*	*10 kyr*	*>78 kyr*

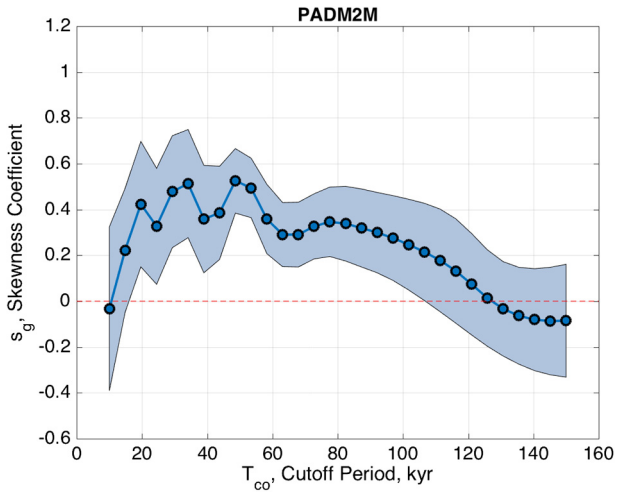

Fig. 3. Geomagnetic skewness coefficient s_g as a function of cutoff period T_{co} for PADM2M. Error bars are ± 1 $\widehat{se}_{jack}$ (standard error estimated using a jackknife method).

We need to know how long a record is needed for unambiguous identification of non-zero geomagnetic skewness coefficient. This was evaluated using sequentially longer distinct test subsets from PADM2M after filtering at $T_{co} = 49$ kyr (see the supplement Section 1.3). We find that a record of at least ~800 kyr, and preferably longer, is needed to confidently observe this asymmetry.

Having established the basic methods for identifying asymmetry in rates of change we turn now to the question of whether the signal found in PADM2M is detected in the marine magnetic anomaly record, either in the time period spanned by PADM2M or during other time intervals.

3. Geomagnetic records from marine magnetic anomalies

The main geomagnetic signal recorded in the oceanic crust is the pattern of reversals that are combined with absolute ages to provide the geomagnetic polarity timescale (GPTS) (Cande and Kent, 1992a, 1995). The seafloor's ability to record the geomagnetic field is affected by the crustal accretion process, and there are a number of potentially confounding variables, including source layer thickness, pattern of lava accumulation, alteration, and the geochemistry of lavas. Generally, we do not expect these processes to be coherent for profiles that are sufficiently separated, so we should be able to see a geomagnetic core-field signal through these. By averaging a significant number of profiles we can be more confident that the coherent signal we observe is of geomagnetic origin.

On smaller spatial and temporal scales than the reversals in the GPTS there are globally coherent anomalies (tiny-wiggles) attributed to either short polarity reversals or intensity fluctuations (Cande and LaBrecque, 1974; Klitgord et al., 1975; Cande and Kent, 1992b). The depth to the magnetization source layer controls the wavelength of the observed anomaly and hence the temporal resolution of the decipherable geomagnetic variations. Sea surface magnetic anomaly profiles are thought to provide a complete record of polarity intervals longer than about 30 kyr (e.g., Cande and Kent, 1992b). Field behavior occurring on timescales shorter than ~30 kyr requires higher-resolution data collected nearer to the source layer. Several studies have found tiny-wiggles that are likely produced by geomagnetic field variations (e.g., Bowers et al., 2001).

It is important to distinguish between the geomagnetic skewness coefficient, s_g, as defined in equation (3) and the terms skewness and anomalous skewness as applied to marine magnetic anomalies. We use geomagnetic skewness to refer to the observed skewed distribution of geomagnetic dipole moment derivatives. The skewness of magnetic anomalies arises from the geometry of the two dimensional source and the direction of the ambient field and remanence. Nonvertical magnetization contrasts, tilting of the magnetization source or systematic changes in geomagnetic intensity may further modify the anomaly shape and this additional contribution is termed anomalous skewness. Although both the source geometry and anomalous skewness may affect our estimate of geomagnetic skewness, we find that the uncertainty associated with these effects is small (Supplemental Section 2.2).

The presence of a saw-toothed pattern (slow decay and more rapid rebound of paleointensity about a reversal) was tested in marine magnetization models (Westphal and Munschy, 1999), and tested as a cause of anomalous marine magnetic anomaly skewness (Dyment and Arkani-Hamed, 2005). These studies did not find the saw-toothed intensity pattern fit their seafloor magnetization models. The three marine magnetic anomaly surveys we examine here are from fast-spreading ridges where anomalous skewness is less pronounced.

3.1. *East Pacific Rise at* 19°–20°*S*

We reanalyze the 0–780 ka near-bottom magnetic anomalies from 19°–20°S of the East Pacific Rise (EPR) discussed by Gee et al. (2000) (Fig. 4). We will refer to this record as "EPR 19°S". These near-bottom anomalies show some similarities with stacked sedimentary relative-paleointensity sequences, and also with the past 50 kyr of absolute-paleointensities from archeomagnetic and volcanic material (Gee et al., 2000). Absolute paleointensities determined from submarine basaltic glass collected at the same study area of the EPR also parallel the near-ridge magnetization values, providing additional support for the importance of geomagnetic intensity fluctuations in modulating crustal magnetization (Gee et al., 2000). Eight anomaly profiles recorded over the faster-spreading eastern flank (76 mm/yr east flank, 142 mm/yr full spreading rate) of the EPR at 19°–20°S were upward continued to a level surface at 2.57 km depth, stacked, and then inverted for magnetization. To upward continue the anomalies, which were measured on an uneven track of the magnetometer above the seafloor, we used the method described in Parker and Klitgord (1972) with 20 line segments to represent the variable-elevation magnetometer track. We stacked the anomalies using the ridge and the Brunhes–Matuyama boundary as the only tie points (Fig. 5a). We inverted the stack of anomalies for the magnetization of a 500 m thick source layer with constant magnetization direction (with inclination determined from the present day latitude) using the two-dimensional Fourier inversion method of Parker and Huestis (1974) (Fig. 5b). Cosine-taper high and low-pass filters reduce the effect of noise at high and low wavenumbers that is amplified during the inversion. To pick the filter parameters (Table S2) we explored a range of magnetization solutions, balancing RMS misfit between the measured and forward modeled anomalies and the $\ell 1$ norm of the magnetization solution (see supplementary Section 2.2 for details).

Similarities between EPR 19°S near-bottom anomalies and PADM2M are evident in Figs. 5b and c and indicate that geomagnetic intensity fluctuations are recorded in the seafloor magnetization. However, the maximum coherence, computed with a multitaper method, between these two records (Fig. 5d) is about 0.5 at long periods (red line) and falls at periods shorter than ~50 kyr (red line coherence falls below the green line 95% confidence level). This modest coherence is to be expected from the relatively low magnetic field strength and shallow inclination associated with anomalies recorded at this low latitude and is evident also in the low between-line coherence in Fig. 4b. The extrusive

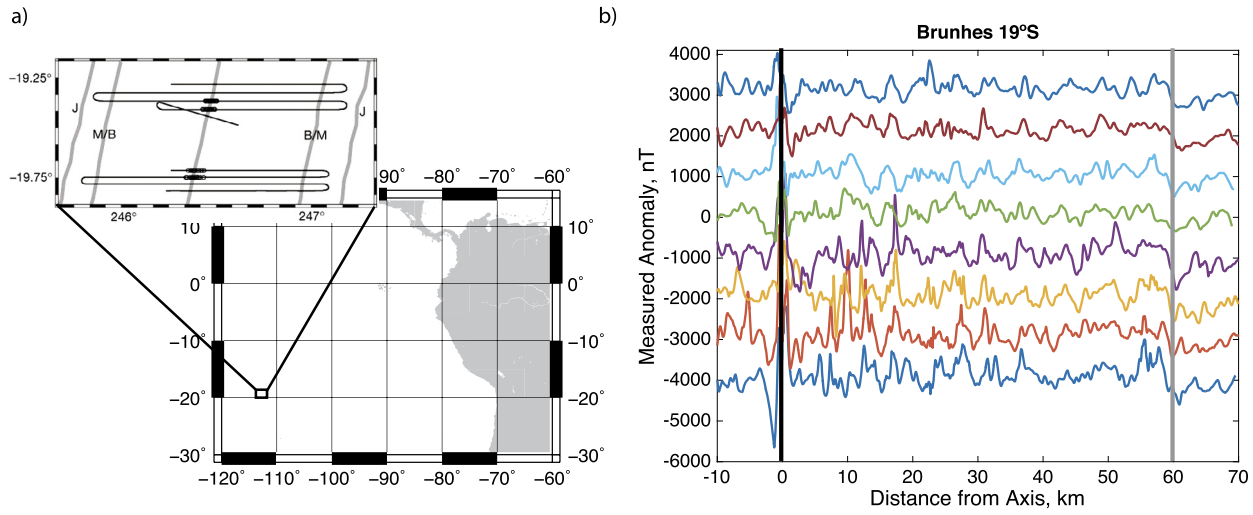

Fig. 4. Brunhes near-bottom marine magnetic anomalies from southern East Pacific Rise (EPR) (Gee et al., 2000) at 19°S. a) Location map modified from Gee et al. (2000). b) Measured near-bottom anomaly profiles from the eastern ridge flank, offset by 1000 nT for clarity. The ridge axis is marked with a black vertical line, and the Brunhes–Matuyama boundary is marked by a grey vertical line.

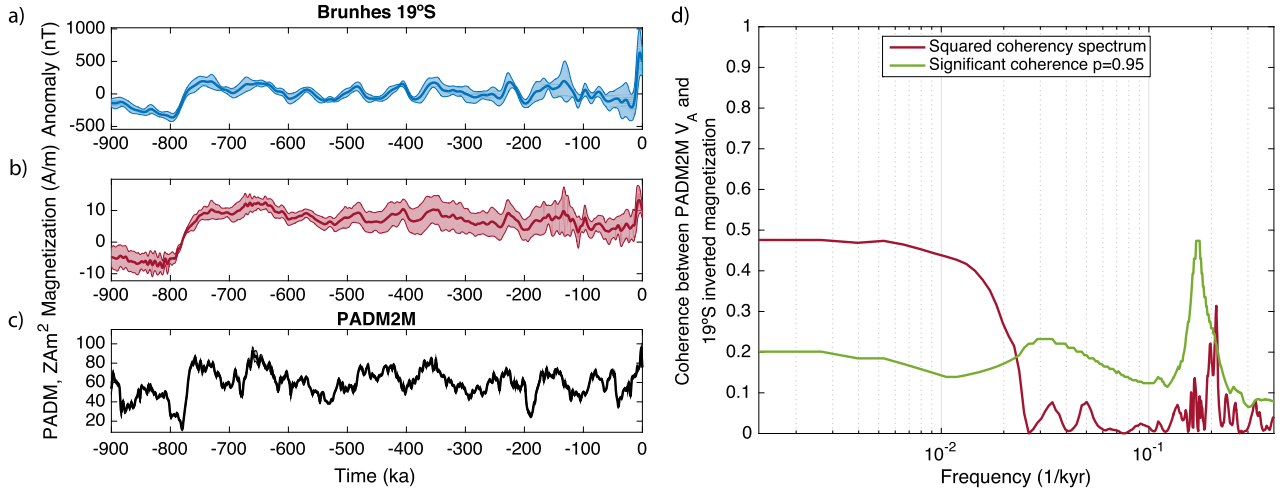

Fig. 5. 19°S EPR Brunhes marine magnetic anomaly. a) Upward continued (to 2.57 km or about 400 m above seafloor) and stacked anomaly, b) inverted magnetization solution, c) PADM2M for comparison. Error bars in panels a, b, and c are ±1 standard error estimated using a jackknife method. Note: the x-axes in panels a, b, and c are age instead of distance, and therefore the anomaly is reflected compared to Fig. 4b. d) Coherence between 0–780 ka 19°S marine magnetic anomaly record and 0–780 ka of PADM2M in red. Green line indicates the level below which no significant coherence can be inferred at the 95% confidence level. See supplementary Section 2 for details of the anomaly processing and inversion. (For interpretation of the references to color in this figure legend, the reader is referred to the web version of this article.)

layer, thought to represent the dominant source of the anomalies, accumulates over a spatial scale of 2–3 km (e.g., Carbotte et al., 1997) and crustal accretion processes may obscure any coherent signal at shorter periods (<25–40 kyr). Indeed, variations in the pattern of crustal accretion may substantially reduce between-line coherence of nearby anomaly profiles (see supplementary Section 3 material).

We repeat the low-pass filter analysis described in Section 2 to determine $s_g(T_{co})$, the geomagnetic skewness coefficient as a function of the filter cutoff period for this stacked magnetization solution. Departures of s_g from zero are statistically significant at periods below 25 kyr and above 39 kyr, $s_g = 1.1 \pm 0.4$ at $T_{co} =$ 15 kyr and $s_g = 0.4 \pm 0.3$ at $T_{co} = 49$ kyr, as shown in Fig. 6 and reported in Table 1. We examine this outcome in greater detail in the Discussion section.

3.2. *Pacific Antarctic Ridge* 51°S

A limited number of near-bottom anomaly records from the Pacific Antarctic Ridge (PAR) provide a much longer geomagnetic field record that may also be used to assess asymmetry. The PAR has been spreading at a relatively uniform half-rate of 42.6 mm/yr for the past 10 Ma (Klitgord et al., 1975). Three near-bottom profiles were collected over the PAR at 51°S during the Southtow Expedition Leg 2 in 1972 (Figs. 7a, b). We will refer to this record as "PAR 51°S". The longest of these lines (traversing both flanks out to anomaly C3n.4n, ~5.2 Myr) was used by Klitgord et al. (1975) in a study of transition zone widths and the central anomaly high at the mid-ocean ridge in the Pacific. The other two near-bottom profiles were recovered from archival tapes providing the total of three lines analyzed here. Although the overall velocity of the eastern flank of the PAR profile is the same as the western flank it exhibits erratic spreading that Klitgord et al. (1975) attribute to ridge jumps. We only used the three profiles from the western flank of the PAR because there were more abundant and consistent data there. We upward continued the three lines to a level track (at 2.1 km depth), stacked them using polarity reversals as tie points (Fig. 7c), and then inverted for magnetization (Fig. 7d). At the polarity boundaries we flip the sign of the magnetization during reversed intervals so that positive slopes correspond with times of

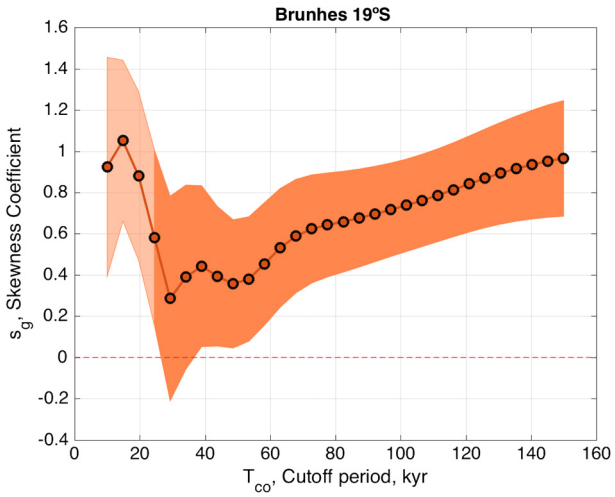

Fig. 6. Geomagnetic skewness coefficient as a function of cutoff period $s_g(T_{co})$ for Brunhes-age anomalies from the EPR near 19°S. Error bars are $\pm 1\ \widehat{se}_{jack}$. The lighter orange shading over cutoff periods <25 kyr indicates the timescale associated with the transition zone width of 1.8 km (Sempere et al., 1987). (For interpretation of the references to color in this figure legend, the reader is referred to the web version of this article.)

field growth and negative slopes decay. We repeat the low-pass filtering and jackknife error analyses described above to estimate $s_g(T_{co})$. Because of the slow survey speeds needed for near-bottom surveys, the 0–5.2 Ma 51°S PAR record $s_g(T_{co})$ is represented by only two long lines (and a third shorter line), resulting in large uncertainty estimates. Nonetheless, the overall pattern of geomagnetic skewness coefficient is positive and significantly greater than zero for cutoff periods above 78 kyr, and the sense of geomagnetic skewness coefficient is also similar to that of PADM2M at shorter periods although not significantly different from zero (Fig. 7e and Table 1). Similar to the result from 19°S (Fig. 6) at long periods (>100 kyr) s_g is significantly greater than zero, unlike PADM2M (Fig. 3).

3.3. Northeast Pacific Chron C5

Perhaps the most robust and best documented near-bottom record of geomagnetic field variations is from the northeast Pacific. Near-bottom magnetic anomaly data from chrons C4Ar–C5r (9.3–11.2 Ma) in the northeast Pacific provide the opportunity to examine whether the asymmetry in the field growth/decay noted over the past few million years is a more general feature of the field. Normal polarity chron C5n.2n is one of the longest periods (~1 Myr) of mostly single polarity with a set of globally coherent tiny-wiggles observed in sea-surface anomaly data (Cande and LaBrecque, 1974). Roberts and Lewin-Harris (2000) presented a

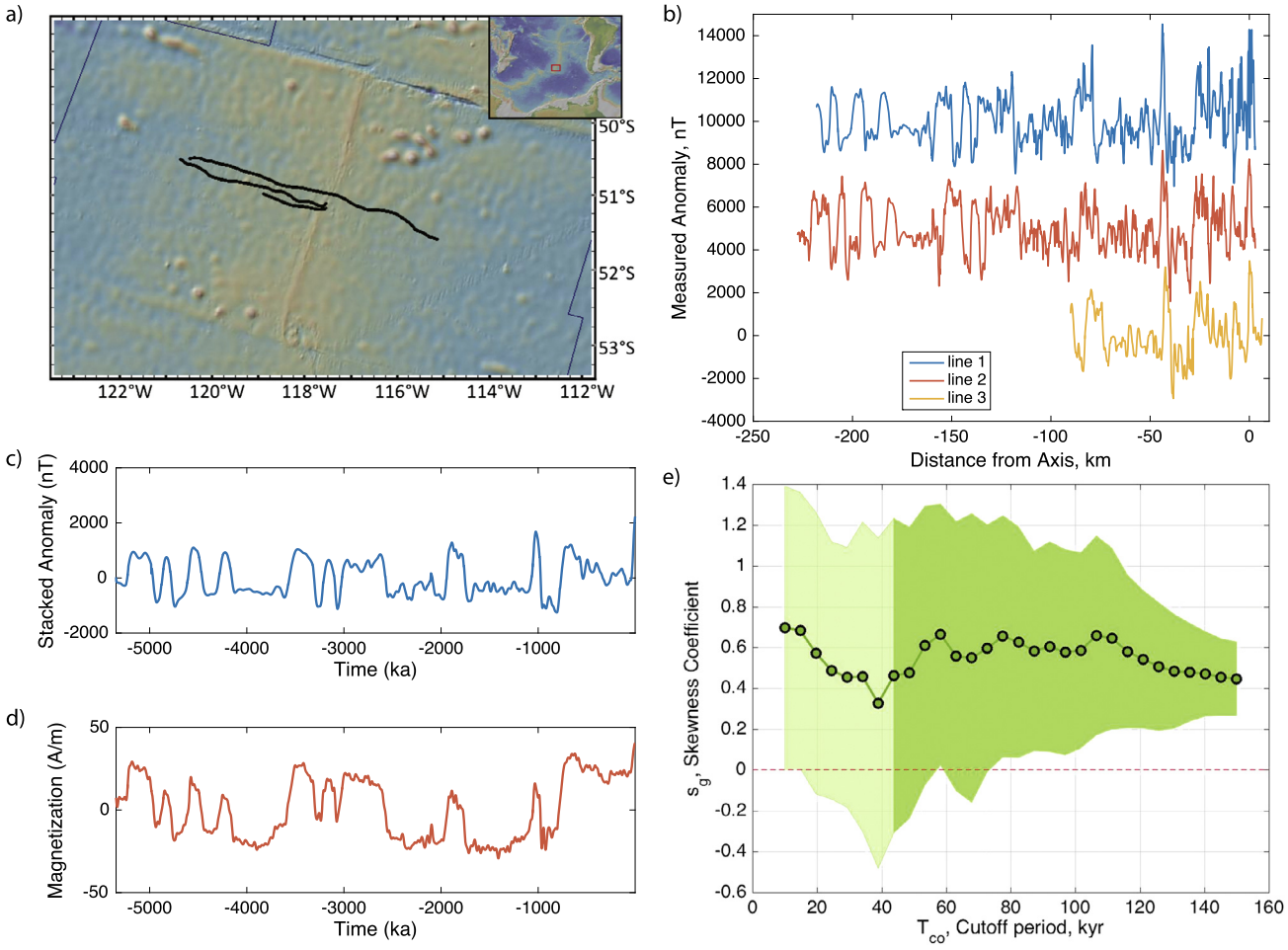

Fig. 7. Pacific Antarctic Ridge near-bottom anomaly data (Klitgord et al., 1975). a) Survey map with isochrons for anomaly 5 (10.9 Ma) and shaded topography. b) Measured anomalies from the eastern side of the ridge offset by 5000 nT for clarity. c) Stacked anomaly after polarity reversal locations were picked. d) Magnetization solution. e) Geomagnetic skewness coefficient s_g as a function of cutoff period T_{co}. Error bars are $\pm 1\ \widehat{se}_{jack}$. The lighter green shading over cutoff periods <44 kyr indicates the timescale associated with the transition zone width of 2.0 km (Klitgord et al., 1975). (For interpretation of the references to color in this figure legend, the reader is referred to the web version of this article.)

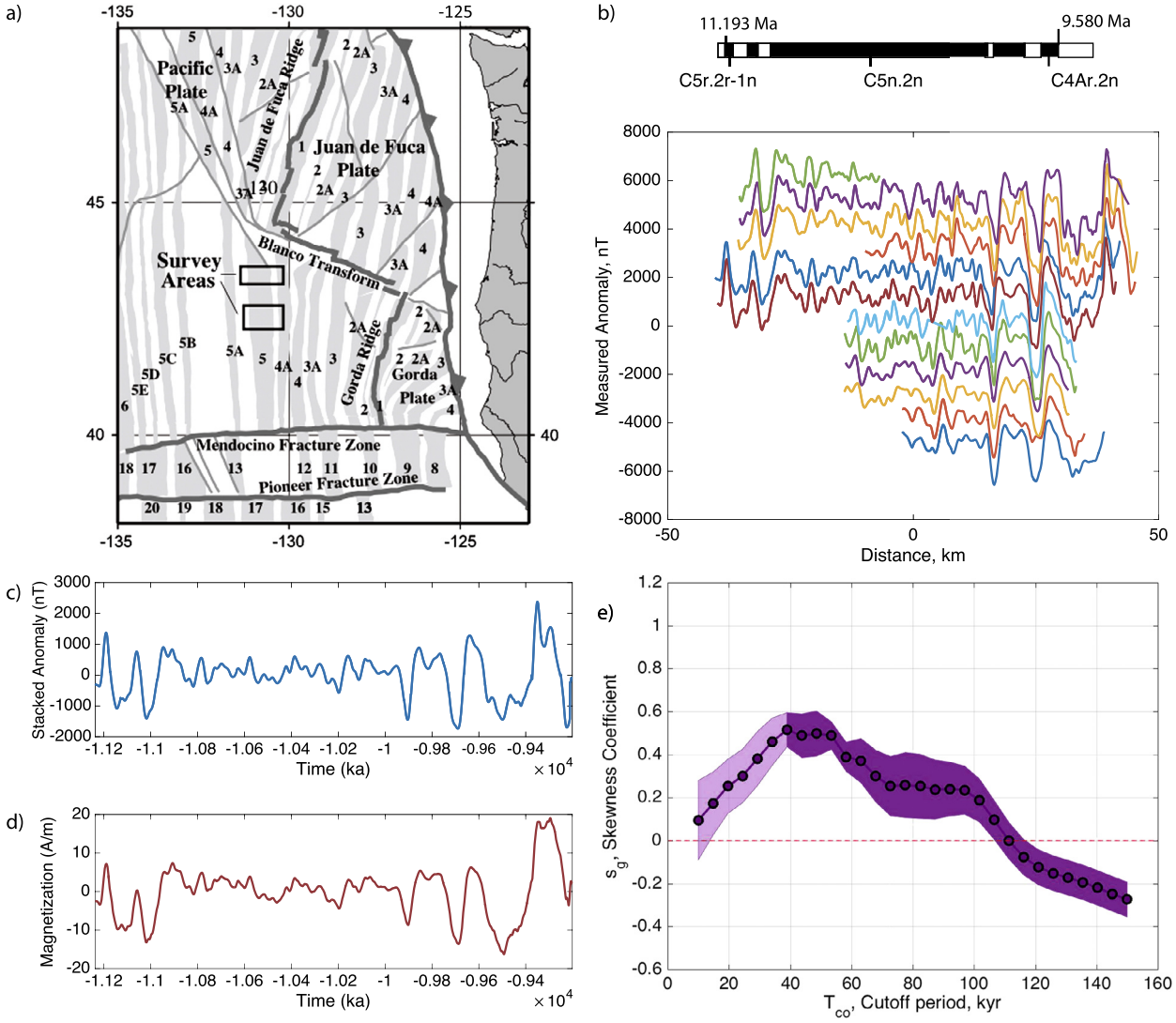

Fig. 8. Northern Pacific chron C5 near-bottom anomaly data (Bowers et al., 2001). a) Survey map modified from Bowles et al. (2003). b) Measured anomalies offset by 1000 nT for clarity with polarity timescale. c) Stacked anomaly after polarity reversal location were picked see text for details. d) Magnetization solution. e) Geomagnetic skewness coefficient s_g as a function of cutoff period T_{co}. Error bars are $\pm 1\ \widehat{se}_{jack}$. The lighter purple shading over cutoff periods <39 kyr indicates the timescale associated with the transition zone width of 1.7 km (Bowers et al., 2001). (For interpretation of the references to color in this figure legend, the reader is referred to the web version of this article.)

Miocene magnetostratigraphic record from ODP Site 884 in the NW Pacific and reported three reversed polarity intervals within C5n.2n. They calculated the durations of these reversed intervals as 6, 26, and 28 kyr. While the shortest (6 kyr) would be poorly represented in sea-surface anomalies (and might be unrecognized), reversed polarity intervals of 26–28 kyr should be readily recognized in near-bottom anomaly profiles and in many sea surface profiles. In another sedimentary record, South Atlantic ODP Site 1092, with a higher sedimentation rate of ~3 cm/kyr (vs ~1 cm/kyr at ODP Site 887) there is evidence that three of the cryptochrons within chron C5n.2n may be excursions (Evans et al., 2007). Bowers et al. (2001) used the complex character of the near-bottom anomalies to argue that the tiny-wiggles in chron C5n.2n were formed by intensity fluctuations rather than short reversals. Bowles et al. (2003) showed that in the North Pacific the tiny-wiggles are highly correlated with an independent record of chron C5 intensity, sedimentary RPI (ODP Site 887) and they found no evidence of reversed polarity intervals within chron C5n.2n.

Twelve near-bottom anomaly lines measured at two survey areas separated by up to ~120 km (eight at the southern area centered at 42°30′N, and four at the northern area centered at 43°30′N) show high between-line coherence as expected at this higher latitude (Fig. 8), and are also well correlated with a single long line covering anomaly 5 from the west flank of the EPR at 19°S (Bowers et al., 2001). We will refer to this record as "chron C5 43°N". Crust in the area is generated at a half spreading rate of 42 mm/yr. Here we start with the raw magnetic anomaly measurements (there was no need to upward continue because data were acquired on a horizontal plane) (Fig. 8b), stack the anomalies (Fig. 8c), and invert for magnetization (Fig. 8d). We use the location of reversals as tie points to stack the lines. One or more brief excursions or reversed polarity intervals may be present within C5n.2n. However, there was no discernible impact on our magnetization interpretation. Accordingly, we have treated it as a long normal polarity period. The reversals are located by iteratively adjusting the polarity boundaries and sigma value (reversal width reflecting spillover of lavas) to minimize the misfit between the measured and forward modeled anomalies (see supplement Section 2). We perform the same analysis as above for $s(T_{co})$. There is significant asymmetry in the ranges of $T_{co} = 15$–107 kyr with a maximum of $s_g = 0.5 \pm 0.1$ at $T_{co} = 39$ kyr (Fig. 8e and Table 1).

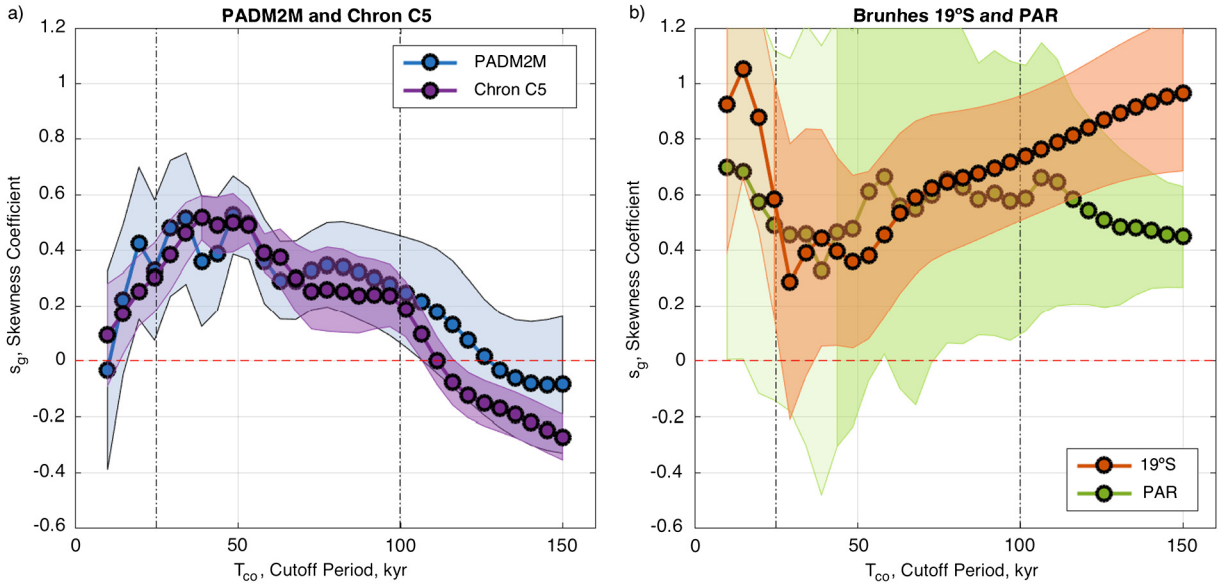

Fig. 9. Comparison of geomagnetic skewness coefficient s_g as a function of cutoff period T_{co} between PADM2M and the three near-bottom marine magnetization studies discussed above. Black dot-dashed vertical lines delineate the three period ranges we compare: short ($T_{co} < 25$ kyr), intermediate ($T_{co} = 25-100$ kyr), and long periods ($T_{co} > 100$ kyr). a) The $s_g(T_{co})$ patterns of PADM2M and chron C5 43°N record agree at all periods. b) The EPR 19°S and PAR 51°S records have positive s_g, but their $s_g(T_{co})$ patterns are different from PADM2M and the chron C5 anomaly record.

4. Discussion

All three of the near-bottom marine magnetization records we analyze here display asymmetry between growth and decay rates in the same sense as PADM2M over at least part of the frequency range studied. We compare the results of the three seafloor magnetization records with PADM2M over three period ranges: short period ($T_{co} < 25$ kyr), intermediate period ($T_{co} = 25-100$ kyr), and long period ($T_{co} > 100$ kyr) (as indicated by the black dot-dashed vertical lines in Fig. 9). Based on the number of profiles and between-line coherence we consider the chron C5 43°N record to be the most reliable of the three near-bottom marine magnetic anomaly records we examined.

The chron C5 43°N record has remarkably high between-line coherence and the $s_g(T_{co})$ (Fig. 9a) results agree remarkably well with PADM2M at all three periods. An important feature of the chron C5 43°N magnetization stack is the data were collected from two survey areas separated by ∼120 km. While this stack would still be considered a regional record it is encouraging that it displays a similar $s_g(T_{co})$ signal to PADM2M, which is a global record. This same general asymmetry is present when the two survey areas are analyzed separately, though the two patterns differ at $T_{co} <\sim 40$ kyr (see supplementary Section 4 for details).

The EPR 19°S and PAR 51°S records have positive geomagnetic skewness coefficient in the intermediate period (significantly different from zero above 39 kyr for the EPR 19°S and above 78 kyr for the PAR 51°S) that parallels that of PADM2M and the chron C5 43°N, but their patterns of $s_g(T_{co})$ differ at both long and shorter periods (Fig. 9b). At low cutoff periods (10–25 kyr) they have positive s_g coefficients while PADM2M and the chron C5 43°N stack are much less skewed. However, the positive s_g at short period seen in the PAR record is not significantly different from zero. Stochastic models of mid-ocean ridge flow accretion indicate that little coherence between anomaly profiles is expected at periods <30 kyr (see supplementary Section 3 for details). This may explain the significant positive s_g seen in the EPR 19°S record at low cutoff periods.

At long periods ($T_{co} > 100$ kyr) all three marine magnetization records show significant geomagnetic skewness coefficient but not all in the same sense. Both the EPR 19°S and PAR 51°S records are positive and the chron C5 43°N record is negative. The chron C5 43°N record signal at long periods agrees with the PADM2M result within their uncertainties. The EPR 19°S record may be too short to constrain the long periods; as we show in the supplement (Section 1.3) at least ∼800 kyr is needed. The standard error on the PAR 51°S $s_g(T_{co})$ pattern is generally larger than the other dataset because the stack is comprised of only two long and one shorter profiles. The EPR 19°S and PAR 51°S records include the ridge and we expect alteration to produce a long period signal in the magnetization, though we find in our stochastic lava accretion models an exponential decay term makes s_g at long T_{co} more negative – the opposite of the EPR 19°S and PAR 51°S long period signal (see supplementary Section 3 for details, Figure S5a).

The similarity of asymmetry in PADM2M and the marine magnetic anomaly records (particularly the chron C5 43°N, but also at intermediate periods for the PAR 51°S and EPR 19°S) suggests that both recording media preserve a record of geomagnetic field asymmetry. Changes in axial dipole strength at the CMB are due to the combined effects of advection and diffusion (Olson and Amit, 2006). Diffusion results in changes that are slow and always decrease the field strength, while changes due to advection are more rapid and can act to increase or decrease the field strength. On long timescales (>100 kyr) we might expect advection and diffusion to be in balance. If changes in the longterm average magnetic field are relatively small, the diffusion and advection terms of the induction equation will balance. This is consistent with absence of significant geomagnetic skewness coefficient signal above 107 kyr in PADM2M.

Our results here confirm that asymmetry between growth and decay rates observed in PADM2M by Ziegler and Constable (2011) is significant and that it is recorded by seafloor magnetization as well as sediments. When fluctuations faster than 15 kyr are filtered out, both PADM2M and our best quality marine magnetization record (the chron C5 43°N dataset) show geomagnetic skewness of the distribution of their rates of change with a peak at ∼40–50 kyr. We interpret this as the signature of diffusion in the axial dipole. To better understand the physical processes driving this asymmetric growth and decay of the dipole we need information about the geomagnetic field morphology at higher spatial resolution than the ADM. The asymmetry between growth and de-

cay rates may provide a valuable criterion for evaluating whether geodynamo simulations are Earth-like. The dynamics of simulations in which the dipole field spends more time decaying than growing and the mean growth is stronger than the mean decay rate can then be examined. For example, on advective timescales reverse flux patches moving from the equatorial region to the poles will weaken the ADM. Similarly, intense normal patches moving from the equator to the poles would increase the ADM. Diffusion will result in overall decreases in field strength (Olson and Amit, 2006).

5. Conclusions

From this study we draw three main conclusions:

1. We parameterize the asymmetry between growth and decay rates in PADM2M in terms of geomagnetic skewness coefficient s_g. The asymmetry is a robust feature and peaks when fluctuations faster than 49 kyr are filtered out.
2. This asymmetry is a feature of geomagnetic field behavior. The fact that it is found in seafloor magnetization as well as the predominantly sedimentary records of PADM2M, indicates it is not a product of the recording processes.
3. This asymmetry is present during two distinct time intervals (0–2 Ma and 9.3–11.2 Ma), and that suggests it is a fundamental feature of secular variation.

The timescale of the most skewed distribution of derivatives in PADM2M and the chron C5 43°N dataset (∼40–50 kyr) is similar to the characteristic diffusion dipole decay timescale of the outer core. This does not provide a direct link to the physical mechanism for this behavior, however, it does provide a new observational criterion for comparing Earth's magnetic field to those produced by geodynamo simulations. It is also useful to know that at least ∼800 kyr of ADM data is needed to make this analysis, which corresponds to ∼4 non-dimensional diffusion times for geodynamo simulations. By studying geodynamo simulations we can assess the outer core flow structures and behaviors that produce this magnetic field behavior. Our study also demonstrates the utility of examining near-bottom marine magnetic anomaly data for geomagnetic field behavior beyond just reversal records.

6. Data availability

PADM2M is available through the EarthRef.org Digital Archive (ERDA) [http://earthref.org/ERDA/1138/]. MGD77 files (and other data) for the near bottom surveys may be found on the SIO Geological Data Center database [http://gdc.ucsd.edu/index.php] (cruise IDs: WEST15MV, SOTW02WT, PANR06MV). Magnetization solutions used in this study and the raw near-bottom magnetics measurements for the PAR are available through ERDA [http://earthref.org/ERDA/2208/].

Acknowledgements

The authors thank Stephen Miller for providing a tape of the Southtow Leg 2 dataset, Steve Cande for helpful discussions, and Leah Ziegler for providing the jackknife resampled PADM2M models. This work was funded by the NSF CSEDI program grant number EAR 1065597. Location maps were drafted using GMT (Wessel et al., 2013) and GeoMapApp (http://www.geomapapp.org/). The authors thank two anonymous reviewers, whose thorough and helpful reviews improved the quality of this manuscript.

Appendix A. Supplementary material

Supplementary material related to this article can be found online at http://dx.doi.org/10.1016/j.epsl.2017.03.020.

References

Backus, G., Parker, R.L., Constable, C., 1996. Foundations of Geomagnetism. Cambridge University Press, New York, NY, pp. 200–204.

Bowers, N.E., Cande, S.C., Gee, J.S., Hildebrand, J.A., Parker, R.L., 2001. Fluctuations of the paleomagnetic field during chron C5 as recorded in near-bottom marine magnetic anomaly data. J. Geophys. Res., Solid Earth 106 (B11), 26379–26396. http://dx.doi.org/10.1029/2001JB000278.

Bowles, J., Tauxe, L., Gee, J., McMillan, D., Cande, S., 2003. Source of tiny wiggles in Chron C5: a comparison of sedimentary relative intensity and marine magnetic anomalies. Geochem. Geophys. Geosyst. 4 (6), 1049. http://dx.doi.org/10.1029/2002GC000489.

Cande, S.C., Kent, D.V., 1992a. A new geomagnetic polarity time scale for the Late Cretaceous and Cenozoic. J. Geophys. Res., Solid Earth 97 (B10), 13917–13951. http://dx.doi.org/10.1029/92JB01202.

Cande, S.C., Kent, D.V., 1992b. Ultrahigh resolution marine magnetic anomaly profiles: a record of continuous paleointensity variations? J. Geophys. Res. 97 (B11), 15075–15083. http://dx.doi.org/10.1029/92JB01090.

Cande, S.C., Kent, D.V., 1995. Revised calibration of the geomagnetic polarity timescale for the Late Cretaceous and Cenozoic. J. Geophys. Res., Solid Earth 100 (B4), 6093–6095. http://dx.doi.org/10.1029/94JB03098.

Cande, S.C., LaBrecque, J.L., 1974. Behaviour of the Earth's palaeomagnetic field from small scale marine magnetic anomalies. Nature 247 (5435), 26–28. http://dx.doi.org/10.1038/247026a0.

Carbotte, S.M., Mutter, J.C., Xu, L., 1997. Contribution of volcanism and tectonism to axial and flank morphology of the southern East Pacific Rise, 17°10′–17°40′S, from a study of layer 2A geometry. J. Geophys. Res., Solid Earth 102 (B5), 10165–10184. http://dx.doi.org/10.1029/96JB03910.

Dyment, J., Arkani-Hamed, J., 2005. Marine magnetic anomalies, oceanic crust magnetization, and geomagnetic time variations. Presented at the Fall meeting of the American Geophysical Union, San Francisco. Abstract GP33B-02.

Evans, H.F., Westerhold, T., Paulsen, H., Channell, J.E., 2007. Astronomical ages for Miocene polarity chrons C4Ar–C5r (9.3–11.2 Ma), and for three excursion chrons within C5n.2n. Earth Planet. Sci. Lett. 256 (3), 455–465. http://dx.doi.org/10.1016/j.epsl.2007.02.001.

Gee, J.S., Cande, S.C., Hildebrand, J.A., Donnelly, K., Parker, R.L., 2000. Geomagnetic intensity variations over the past 780 kyr obtained from near-seafloor magnetic anomalies. Nature 408 (6814), 827–832. http://dx.doi.org/10.1038/35048513.

Holme, R., 2015. Large-scale flow in the core. In: Treatise on Geophysics, vol. 8, pp. 91–113 (Chapter 4).

Klitgord, K., Huestis, S., Mudie, J., Parker, R., 1975. An analysis of near-bottom magnetic anomalies: sea-floor spreading and the magnetized layer. Geophys. J. Int. 43 (2), 387–424. http://dx.doi.org/10.1111/j.1365-246X.1975.tb00641.x.

Kok, Y.S., Tauxe, L., 1996a. Saw-toothed pattern of relative paleointensity records and cumulative viscous remanence. Earth Planet. Sci. Lett. 137 (1), 95–99. http://dx.doi.org/10.1016/0012-821X(95)00210-4.

Kok, Y.S., Tauxe, L., 1996b. Saw-toothed pattern of sedimentary paleointensity records explained by cumulative viscous remanence. Earth Planet. Sci. Lett. 144 (3), E9–E14. http://dx.doi.org/10.1016/S0012-821X(96)00175-6.

Olson, P., Amit, H., 2006. Changes in Earth's dipole. Naturwissenschaften 93 (11), 519–542. http://dx.doi.org/10.1007/s00114-006-0138-6.

Parker, R., Huestis, S., 1974. The inversion of magnetic anomalies in the presence of topography. J. Geophys. Res. 79 (11), 1587–1593. http://dx.doi.org/10.1029/JB079i011p01587.

Parker, R.L., Klitgord, K.D., 1972. Magnetic upward continuation from an uneven track. Geophysics 37 (4), 662–668. http://dx.doi.org/10.1190/1.1440289.

Parks, T., McClellan, J., 1972. Chebyshev approximation for nonrecursive digital filters with linear phase. IEEE Trans. Circuit Theory 19 (2), 189–194. http://dx.doi.org/10.1109/TCT.1972.1083419.

Pozzo, M., Davies, C., Gubbins, D., Alfè, D., 2012. Thermal and electrical conductivity of iron at Earth's core conditions. Nature 485 (7398), 355–358. http://dx.doi.org/10.1038/nature11031.

Roberts, A.P., Lewin-Harris, J.C., 2000. Marine magnetic anomalies: evidence that 'tiny wiggles' represent short-period geomagnetic polarity intervals. Earth Planet. Sci. Lett. 183 (3), 375–388. http://dx.doi.org/10.1016/S0012-821X(00)00290-9.

Roberts, A.P., Tauxe, L., Heslop, D., 2013. Magnetic paleointensity stratigraphy and high-resolution Quaternary geochronology: successes and future challenges. Quat. Sci. Rev. 61, 1–16. http://dx.doi.org/10.1016/j.quascirev.2012.10.036.

Sempere, J.-C., Macdonald, K.C., Miller, S.P., Shure, L., 1987. Detailed study of the Brunhes/Matuyama reversal boundary on the East Pacific Rise at 19°30′S: im-

plications for crustal emplacement processes at an ultra fast spreading center. Mar. Geophys. Res. 9 (1), 1–23. http://dx.doi.org/10.1007/BF00338248.

Tauxe, L., Yamazaki, T., 2015. Paleointensities. In: Treatise on Geophysics, vol. 5, pp. 461–509 (Chapter 13).

Valet, J.-P., Fournier, A., 2016. Deciphering records of geomagnetic reversals. Rev. Geophys. 54 (2), 410–446. http://dx.doi.org/10.1002/2015RG000506.

Valet, J.-P., Meynadier, L., 1993. Geomagnetic field intensity and reversals during the past four million years. Nature 366 (6452), 234–238. http://dx.doi.org/10.1038/366234a0.

Valet, J.-P., Meynadier, L., Guyodo, Y., 2005. Geomagnetic dipole strength and reversal rate over the past two million years. Nature 435 (7043), 802–805. http://dx.doi.org/10.1038/nature03674.

Wessel, P., Smith, W.H., Scharroo, R., Luis, J., Wobbe, F., 2013. Generic mapping tools: improved version released. Eos, Trans. Am. Geophys. Union 94 (45), 409–410. http://dx.doi.org/10.1002/2013EO450001.

Westphal, M., Munschy, M., 1999. Saw-tooth pattern of the Earth's magnetic field tested by magnetic anomalies over oceanic spreading ridges. C. R. Acad. Sci. Ser. IIA Earth Planet. Sci. 329 (8), 565–571.

Ziegler, L., Constable, C., 2011. Asymmetry in growth and decay of the geomagnetic dipole. Earth Planet. Sci. Lett. 312 (3), 300–304. http://dx.doi.org/10.1016/j.epsl.2011.10.019.

Ziegler, L., Constable, C., Johnson, C., Tauxe, L., 2011. PADM2M: a penalized maximum likelihood model of the 0–2 Ma palaeomagnetic axial dipole moment. Geophys. J. Int. 184 (3), 1069–1089. http://dx.doi.org/10.1111/j.1365-246X.2010.04905.x.